Interaction of CO_2 with well-ordered iron sulfide films on Au(111)

Giulia Berti[a,b], Earl M. Davis[a], Helmut Kuhlenbeck[a,*], Hans-Joachim Freund[a]

[a] *Fritz-Haber-Institut der Max-Planck-Gesellschaft, Faradayweg 4-6, 14195, Berlin, Germany*

[b] *Current affiliation: Institut National de la Recherche Scientifique, Centre Énergie Matériaux Télécommunication, 1650 Boulevard Lionel-Boulet, Varennes (Québec) J3X 1S2 Canada*

Abstract

Iron sulfides are important in catalysis because of their abundance on earth and their catalytic activity. In Wächtershäuser's origin of life theory, Fe/Ni sulfide deposits in and near to submarine hydrothermal vents ('black smokers') catalyzed the production of first organic matter, and recent studies have indicated that iron sulfides might be able to activate CO_2 towards conversion into chemicals such as methanol, formic acids and others. Here, we present a study of the interaction of carbon dioxide with well ordered iron sulfide films grown on Au(111). Since the as-prepared film proved to be rather non-reactive to the molecule, possibly because of the layer's sulfide termination, we tried to modify the sulfide's stoichiometry both by exposing it to atomic hydrogen and by adding metallic iron. Hydrogen is able to interact with the sulfur on the surface and to partially remove it, but the resulting surface is still not reactive towards CO_2. X-ray photoemission results show that the addition of metallic iron is detrimental for the quality of the sample, giving rise to the admixture of substrate gold to the layer. Insertion of an FeO blocking layer between the sulfide and the gold substrate allowed the sulfide to become Fe-rich, enhancing its reactivity towards CO_2, but it was not possible to completely prevent diffusion between the FeO layer and the substrate. However, we found that an increased iron content together with the presence of gold was able to activate the layer towards CO_2.

Keywords: CO_2 activation, thin crystalline films, iron sulfide, model catalysis

1. Introduction

Iron sulfides are a group of compounds ubiquitously present in nature, especially in marine systems. They have attracted much attention and have been

*Corresponding author

the object of several studies over the last decades: there are studies of bulk clusters, precipitates [1, 2, 3], and films [4, 5, 6]. Among others, iron sulfide surfaces have been studied in recent years for their reactivity to H_2 in the production of ammonia [7], to water, and CH_3OH [8], just to name a few. The reactivity of iron sulfides to CO_2 has also been a very important topic in the catalysis community, partially because of the origin of life theory of G. Wächtershäuser [9], which is based on the submarine production of simple organic molecules by catalytic sulfide compounds.

As the interest in understanding chemical reactions at the atomic level increases, the detailed control of the surface structure has become of paramount importance. X-ray photoemission spectroscopy (XPS) has already been employed to characterize several Fe-S compounds [4, 10], showing that differences in the surface stoichiometry derived from reconstruction [5] affect the surface reactivity.

In a recent paper [11], we describe a recipe for the growth of iron sulfide thin films on Au(111). Their morphological, structural, and chemical properties were investigated by means of several ultra-high vacuum (UHV) techniques. We could show that the film is well ordered and has a NiAs-type structure with a slightly lower Fe occupancy than Fe_7S_8. The surface of the layer exhibits a (2×2) reconstruction with respects to its 'bulk' lattice. We found the film to be not very reactive to CO_2 or other small molecules which we attribute to its sulfur termination. In this work, we test the reactivity of the *in-situ* grown iron sulfide film to CO_2 by following two different approaches: modifying the surface reactivity by exposure to H_2, and by addition of metallic Fe. In the second case, the insertion of an iron oxide blocking interlayer was needed to prevent loss of iron into the gold substrate.

2. Experimental details

An Au(111) single crystal (MaTecK, 99.999% purity) was used as a substrate for this study. It was cleaned by repeated cycles of Ar-ion sputtering at 3 keV followed by annealing at 1000 K for at least 40 minutes in UHV. The annealing was done by electron bombardment from a filament placed in close proximity of the sample, and the temperature was monitored with a Chromel-Alumel thermocouple spot-welded on the side of the crystal. The effectiveness of the cleaning procedure was tested by low energy electron diffraction (LEED, see Fig. 1a).

Iron sulfide thin films were grown by molecular beam epitaxy (MBE) in a dedicated chamber with a base pressure in the 10^{-10} mbar range, equipped with a quartz microbalance, an Fe evaporator and a sulfur sublimation cell, described elsewhere [11]. The growth was performed with the substrate kept at about 650 K (to allow for film ordering), by evaporating Fe in a reactive sulfur atmosphere at a rate of 0.1 nm/min [11].

FeO monolayers were grown on the clean Au substrate by following a procedure described by Khan and Matranga [12]: first an Fe monolayer was deposited by MBE at room temperature. The oxide was then formed by post-oxidation

via backfilling of the chamber with 3×10^{-7} mbar of molecular O_2 for 500 s with the sample at a slightly elevated temperature (323 K). Eventually, the sample was annealed in vacuum at 700 K for 10 minutes.

Sample characterization was done in an Omicron UHV chamber with a base pressure in the low 10^{-11} mbar range. STM images were acquired in this chamber with an Omicron room temperature STM (STM 1) operated in constant-current mode using home-made electrochemically etched tungsten tips. The WSxM software [13] was used for STM image processing.

The chemical composition of the sample was probed with XPS employing Mg K_α unmonochromatized radiation (photon energy: 1253.6 eV). Photoemitted electrons were collected with an Omicron EA125 hemispherical electron analyzer operated at a pass energy of 20 eV (instrumental resolution: 0.6 eV). Unless the emission angle is given, all of the spectra shown hereafter were acquired in grazing emission geometry: the angle between the sample normal and the axis of the analyzer was set to 70°.

Temperature programmed desorption (TPD) experiments were performed after dosing the gas in a dedicated high-pressure chamber. Data acquisition was then conducted in the analysis chamber. The sample was positioned in front of the quadrupole mass spectrometer (QMS) at a distance of about 1 mm. The head of the QMS was fitted inside a housing with a small aperture in the front [14], and the whole system was connected to a differential pumping stage. The short sample-nozzle distance and the differential pumping ensured that gas desorbing from the sample holder could only contribute weakly to the TPD spectra. TPD spectra were acquired with a constant heating rate of 0.5 K/s.

For the exposure to atomic hydrogen, the chamber was filled with H_2 with pressures in the range of $10^{-8} - 10^{-7}$ mbar, depending on the intended dose. For experiments involving atomic hydrogen, molecular hydrogen was cracked by a glowing tungsten filament operated close to the sample surface.

3. Results

3.1. CO_2 absorption on the pristine surface

Following the procedure described in Ref. [11], an ∼25 nm thick iron sulfide layer was grown on the Au(111) substrate. This resulted in a well ordered layer with sixfold symmetry and a (2×2) surface reconstruction (Fig. 1b).

A series of XPS spectra was measured at different electron emission angles. In this way, it was possible to vary the surface sensitivity, with the largest surface sensitivity obtained at the highest emission angle relative to the surface normal. Carbon, oxygen, and gold could not be detected at all. Fig. 2 shows the ratio between the integrated areas of the Fe $3p$ and the S $2p$ peaks, normalized by the respective relative sensitivity factors, which take into account the cross section of the elements [15].

The graph shows that the Fe/S ratio decreases with increasing emission angle, starting from a value of about 0.43 at 12° and decreasing to a value slightly above 0.1 as 90° is approached. From this we conclude that the sample is

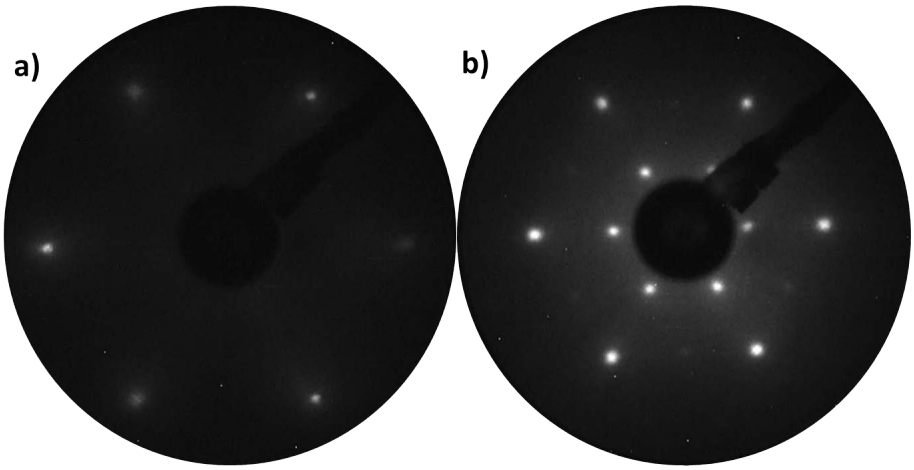

Figure 1: LEED patterns of (a) the Au(111) substrate, and (b) the iron sulfide film recorded with electrons having a kinetic energy of 127 eV. The brightness of both images was digitally enhanced to improve the visibility of the spots.

most probably terminated by a layer with a high sulfur content. This conclusion holds even if the rather large error bar is considered.

The purpose of the present study was to investigate the reactivity of such films with respect to CO_2. CO_2 was dosed in the preparation chamber with the flow adjusted such that the foreline pressure measured with a Pirani gauge near the turbo pump reached a value of 1 mbar. The pressure in the preparation chamber could not be measured directly, but we estimate that it was within the range of 10^{-2} mbar. The pressure was kept for 30 minutes with the sample at room temperature. XPS and TPD data (not shown) did not reveal indications of CO_2 or CO_2-derived molecules at the sulfide surface.

The typical mechanism for CO_2 activation is electron transfer to the molecule[16], which requires the availability of charge which can be transferred at a low energy cost. Therefore we felt that reducing the sulfide might activate it towards the activation of CO_2. Ways to achieve this are removal of sulfur and addition of iron; we followed both directions.

3.2. Surface modification with atomic hydrogen

Several attempts were made to make the film more reactive towards CO_2 by increasing the iron concentration at the surface. One try was to dose atomic hydrogen. Exposure at room temperature did not lead to any detectable effect. Then, H dosing was repeated with the sample kept at 100 K, initially with a dose of 10 L (1 L = 10^{-6} Torr×s). TPD data recorded after dosage of 10 L of hydrogen are shown in Fig. 3.

H_2S, S, and some H_2 are found to desorb. The H_2 trace is rather structureless and one may assume that at least part of the structures are due to desorption from the sample holder. The sharp spikes in the H_2 spectrum are too sharp for

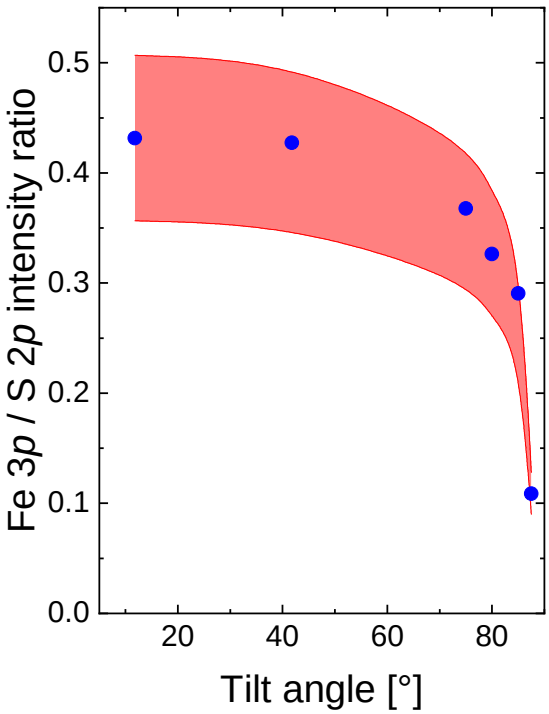

Figure 2: Normalized intensity ratio between Fe 3*p* and S 2*p*. The red area is an estimate of the experimental error.

regular TPD maxima; we attribute them to short sparks related to the high voltage of the sample heater. The H_2S spectrum exhibits a peak at around 250 K, followed by a large shoulder, which extends up to 400 K. The H_2 and S curves exhibit similar structures with the wide shoulder being barely recognizable in the H_2 spectrum. According to the NIST chemistry webbook [17] H_2S should be accompanied by a significant S signal due to cracking of the H_2S molecule in the mass spectrometer, which is probably the origin of the structures in the S spectrum. The structure at ∼250 K in the H_2 spectrum may also be due to this, but also a reaction of the H_2S at the chamber walls, the mass spectrometer surface and the inner walls of the QMS housing are conceivable. H_2S desorption means that the film is reduced by sulfur removal, as intended. However, dosage of CO_2 revealed that the surface was not notably activated – no C- and O-containing species could be detected at the surface with XPS and TPD.

Next, we dosed atomic H in two separate steps. In this "double exposure" experiment, the first dosage step was exposure to H as described above. The sample was then flashed to room temperature (see Fig. 3) in order to desorb adsorbed H and H_2S, thereby freeing surface sites. This was done in order to remove adsorbed hydrogen and H_2S to free sites for further reduction. After cooling down again to 100 K, a second exposure was carried out with the same

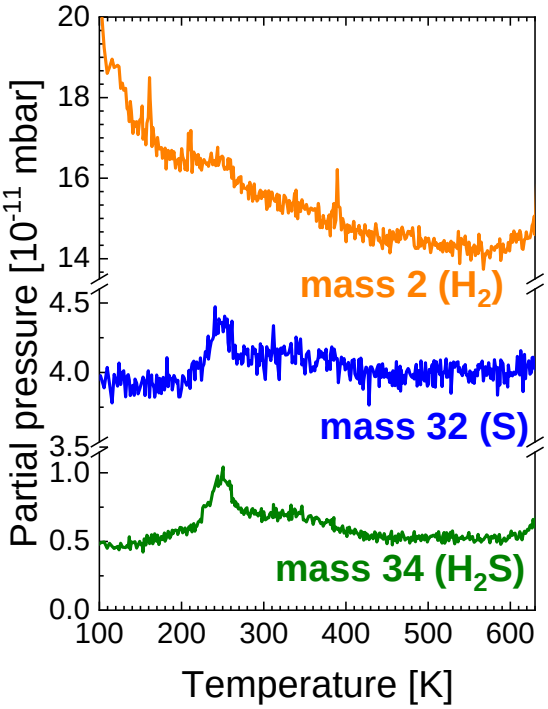

Figure 3: TPD spectra acquired after dosing 10 L of atomic H_2 at 100 K. The masses 34, 32, and 2 were measured for H_2S, S, and H_2, respectively.

parameters (dose, pressure, time) as the first one. Different TPD spectra were acquired for several increasing "double exposure" doses, and the results for H_2S are shown in Fig. 4.

The results show that the amount of H_2S desorbing from the surface increases with increasing hydrogen dose, with the centroid of the desorption curve shifting from ∼250 K to ∼360 K for the highest dose. This demonstrates that the surface is actually modified by the interaction with atomic hydrogen. Consequentially, XPS data recorded after "double exposure" of 10^4 L reveal an increase of the iron concentration (Fig. 5). In addition, Fig. 5 shows that the S $2p$ doublet shifts, with its main peak moving from 161.3 eV to 162.0 eV upon surface reduction by hydrogen. This is most probably due to a modified coordination of the sulfur atoms. Consequently, the binding energy of the Fe $2p$ changes by a similar amount in the opposite direction, from ∼708.15 eV to ∼707.3 eV for the Fe $2p_{3/2}$ peak maximum, indicative of a reduction of the iron atoms.

Davis et al assigned S $2p$ peaks at 161.4 eV and 162.5 eV to fivefold and sixfold coordinated sulfur, respectively [11]. The shift in the binding energy of the S $2p$ peak observed here indicates, that part of the fivefold coordinated sulfur is transformed into sixfold coordinated sulfur, giving additional evidence for an increase of the surface-near iron concentration by the treatment with

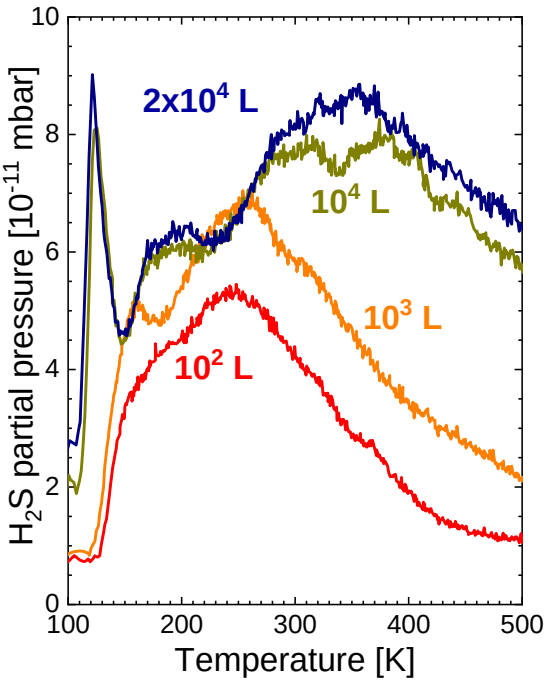

Figure 4: TPD spectra acquired at mass 34 (H_2S) for increasing "double exposure" atomic H doses at 100 K.

atomic hydrogen.

However, even this treatment did not activate the surface with respect to CO_2. Neither carbon nor oxygen could be detected at the surface after CO_2 dosage at room temperature. Note that the surface modification was only possible with atomic H at low temperature, as modification with molecular H_2 proved to be unsuccessful.

3.3. Surface modification by deposition of metallic Fe

In another approach to increase the reactivity towards CO_2, the surface of the pristine FeS_x/Au(111) film was modified by depositing 12 nm of metallic Fe at room temperature. This produced a disordered surface as indicated by the absence of visible spots in the LEED pattern. A subsequent 650 K annealing step was required to order it. However, this step also resulted in the loss of the extra Fe, which appeared to migrate to deeper layers or into the Au(111) substrate, leading to a sulfur-terminated outer layer like it was before the iron deposition step.

Another effect of the annealing step was that gold core levels became visible in XPS spectrum with the Au $4f$ intensity corresponding to roughly 25% of a monolayer (1 ML $\hat{=}$ 1 Au(111) layer). The Au $4f$ signal was larger by a factor of $\approx$2 at normal emission than at grazing emission (Fig. 6), which excludes that

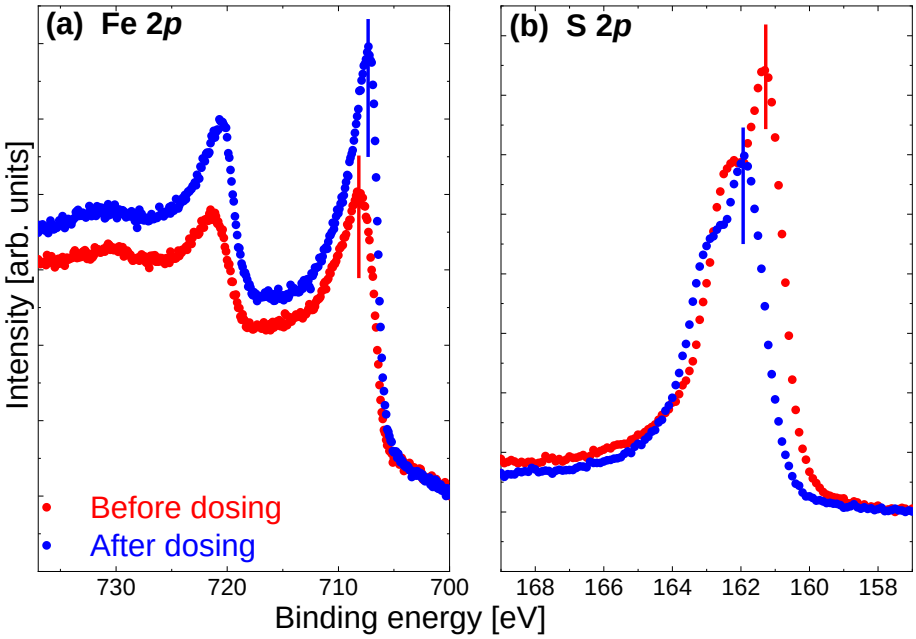

Figure 5: XPS spectra taken in the region of (a) Fe $2p$ and (b) S $2p$ before and after the "double exposure" (10^4 L of atomic hydrogen at 100 K) TPD experiment.

the Au was located at the film surface. Dewetting, gold diffusion into the film as well as thinning of the film are conceivable as reasons for the visibility of the Au $4f$ levels. Dewetting would be compatible with a larger Au $4f$ XPS intensity at normal emission if the holes are deep and small which is not unlikely for thin films. For the case of gold diffusion the XPS data would mean that the gold stays below the surface. For the remaining case, film thinning, one may compute a film thickness of 0.8 nm for an intensity reduction by a factor of 2 when going from normal to grazing emission, a flat layer and an inelastic mean free electron path of 2.3 nm as calculated with the Quases IMFP program [18]. While we cannot exclude that so much iron diffused into the substrate, we consider it unlikely that the film thickness is reduced significantly below the thickness of the pristine film, and therefore the dewetting and diffusion scenarios appears more likely for us.

A comparison of Au $4f$ XPS spectra before and after deposition of metallic iron and annealing (after exposure of the sample to CO_2) is shown in Fig. 7a. In this case small carbon and oxygen signals became visible in the XPS spectra (not shown), but their intensities were too small to allow for a detailed analysis. We estimate that the carbon/oxygen coverages at the surface were in the range of a few percent.

A solution to the iron migration problem was sought in the insertion of a diffusion blocking layer at the interface between the gold substrate and the

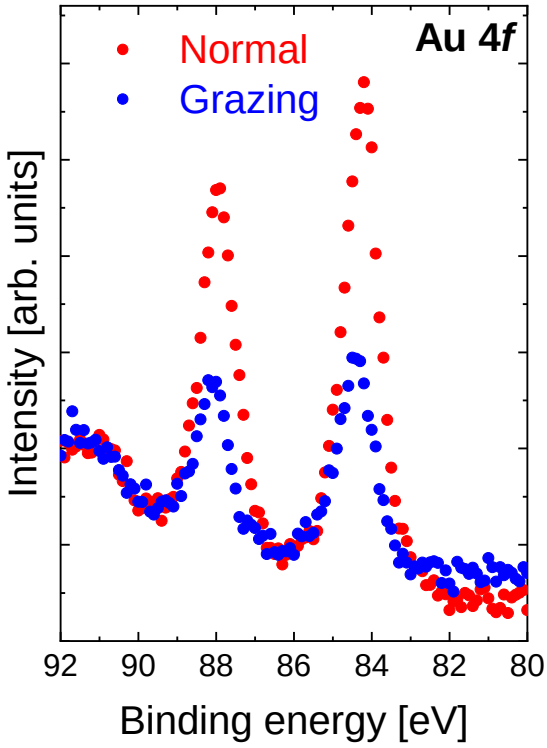

Figure 6: XPS scans of the Au $4f$ region for the sulfide sample after iron deposition and annealing. Red dots: normal angle electron detection; blue dots: grazing angle electron detection.

sulfide film. A tantalum sulfide layer was tried initially, since the corresponding oxide had been efficient in isolating a TiO_2 film in a previous work [19]. However, while the formation of tantalum sulfide was clear from XPS measurements, the film did not block the iron migration and therefore it was disregarded.

After this failure we tested the usability of an FeO interlayer (thickness $\sim$ 1 ML). The idea of using FeO as a template to grow the sulfide film came from a work by Sala *et al.* [20], who employed it to grow Fe_3O_4 layers on Pt(111). FeO monolayers are known to grow well on Pt(111) [21, 22], while the literature of FeO films on Au(111) is scarce. The quality of the FeO monolayers obtained in this work was never perfect, nevertheless it was possible to reduce iron migration into the substrate.

Before sulfide deposition, the FeO layer was characterized with STM and XPS. Fig. 8a shows the morphology of the film at an intermediate stage of growth, with a striped texture well visible in the large scale image. The zoom in the inset exhibits the typical Moiré pattern of the film. This pattern was also observed with LEED.

The Fe $2p$ XPS spectrum in Fig. 8b shows the Fe $2p$ doublet with the 3/2 part

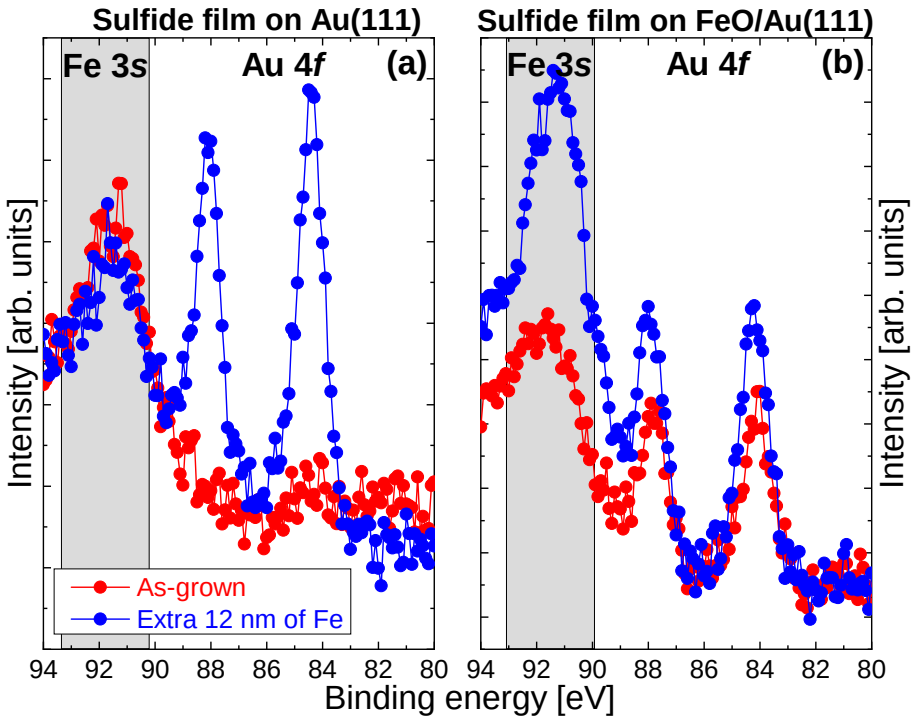

Figure 7: Au $4f$/Fe $3s$ XPS spectra. (a) without, and (b) with a FeO blocking layer at the substrate/film interface before and after Fe deposition and annealing.

of the doublet at 710.1 eV and a shake-up satellite at about 6 eV higher energy. This value is in agreement with that reported in the literature for wüstite (FeO) [23].

A 25 nm thick Fe sulfide was grown on top of the completed FeO/Au(111) layer following the same procedure as without the blocking layer. Also in this case the resulting film was sulfur-terminated and not reactive to CO_2. Then 12 nm of iron were added at room temperature, followed by annealing at 650 K for 10 minutes in UHV, as done before for the film without the blocking layer. In Fig. 7, a comparison of the Au $4f$ and Fe $3s$ peaks before and after Fe deposition and annealing is shown for a film without (panel a) and with a blocking layer (panel b).

The left panel of the figure shows that the intensity of the Au $4f$ is basically zero when the sulfide is grown without the FeO interlayer. However, the Au $4f$ increases notably after Fe deposition and annealing, while the Fe $3s$ intensity is basically unchanged. The situation is different when the FeO layer is present. In this case a small signal coming from the Au $4f$ doublet is already detectable right after sulfide deposition. Its intensity was estimated to correspond to about 5−10% of a monolayer and doesn't change significantly after iron deposition and annealing. Most important, however, is the net increase in Fe $3s$ intensity

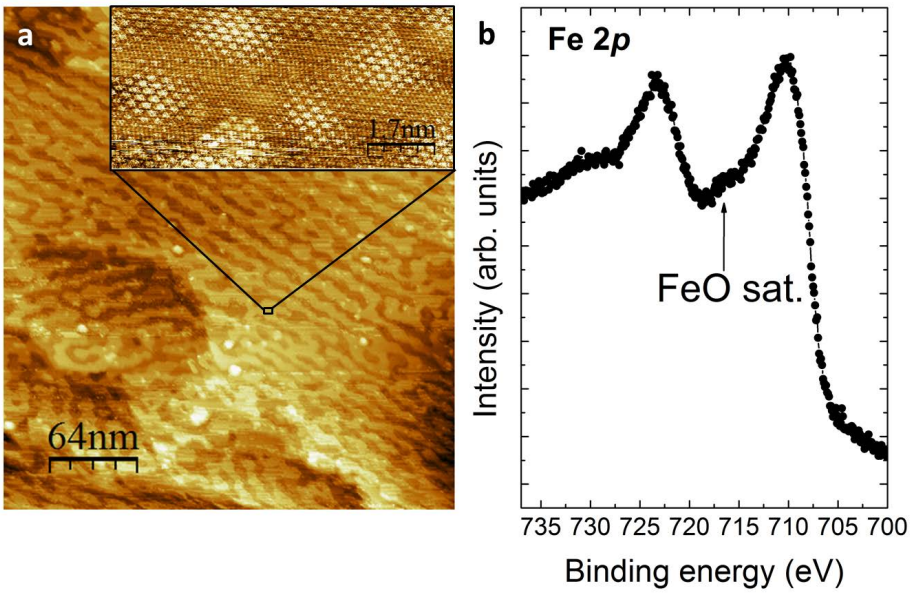

Figure 8: a) STM image of a 0.5 ML FeO film on Au(111). The inset shows an enlarged area of an island (tunneling parameters: $V = 2\,\mathrm{V}$ and $I = 0.1\,\mathrm{nA}$). b) XPS scan of the Fe $2p$ region with the FeO satellite indicated by an arrow.

even after annealing the sample, meaning that the extra Fe was able to change the film stoichiometry. From a surface sensitive XPS spectrum recorded at a detection angle of 70° with respect to the surface normal (not shown here) we estimate that the Fe:S concentration ratio is ∼1.35 within the topmost 7.5 Å of the film. The LEED pattern shows that the (2×2) reconstruction is lifted (Fig. 9b), which again points towards a significant structural change at the surface.

The FeS_x/FeO/Au sample was then exposed to CO_2. A XPS spectrum of the surface reveals the presence of some carbon and oxygen (see Fig. 10), which means that the surface could be activated to chemically interact with carbon dioxide. The weak oxygen trace in the spectrum of the freshly prepared film is probably due to the underlying FeO layer. C1s and O1s XPS spectra measured in normal emission exhibit much weaker peaks than the spectra shown in Fig. 10, which were taken at a grazing emission angle of 70°. This is a clear indication that the C $1s$ and O $1s$ intensities stem from oxygen and carbon species at the surface. The C $1s$ binding energy of 284.0 eV is compatible with the formation of a carbide [24]. The C $1s$/O $1s$ intensity ratio normalized by the relative sensitivity factors is close to 0.5 as expected for CO_2 derived species, with the amount of carbon corresponding to a film with a nominal thickness of 1−2 Å. Interestingly, after 10 minutes of mild annealing (650 K), the XPS signal from carbon vanishes (crosses, Fig. 10a), while only the high energy shoulder of the O $1s$ peak disappears; most of the oxygen remains at the surface. TPD data (not shown) suggest that carbon does not desorb from the surface during the

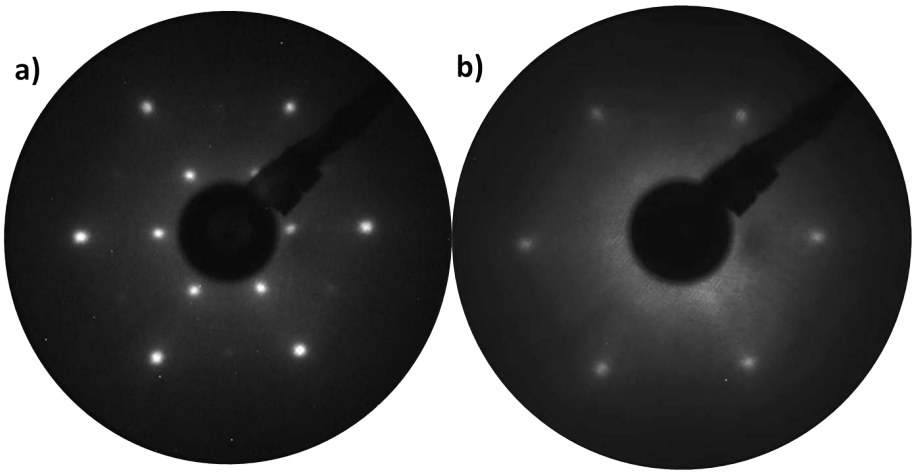

Figure 9: LEED patterns of (a) the Fe sulfide film grown on Au(111), and (b) the Fe sulfide film grown on FeO/Au(111) after the addition of metallic iron and annealing. The brightness of both images was digitally enhanced and the electron energy was 127 eV.

annealing, but is dissolved into the sulfide, while oxygen stays on the surface of the film.

4. Discussion

In an attempt to summarize and discuss, we have performed CO_2 reactivity studies for a number of differently prepared iron sulfide surfaces: The regular, as prepared surface turned out to be unreactive towards CO_2 at all temperatures. Next, the iron sulfide film was exposed to atomic hydrogen, which, as judged by XPS, increased the relative amount of iron in the topmost surface layers by removing some of the sulfur via H_2S formation. This iron rich system turned out to be nonreactive towards CO_2 as well. When iron was added by evaporation and the film was annealed at 650 K, Au was detected via XPS, and a few percent of oxygen and carbon were detected again via XPS, indicating a slight onset of reactivity after CO_2 exposure. To possibly prevent Au from diffusing, the Au surface was covered with an FeO blocking layer before the iron sulfide film was grown. However, Au still showed up in XPS, but the system was unreactive against CO_2 exposure. When iron was evaporated on this system with a subsequent annealing to 650 K, 1-2 monolayers of carbon and oxygen were detected after CO_2 exposure. The highest reactivity is found for the film with the highest iron concentration at the surface, followed by the sample which was exposed to iron, but without the blocking layer, so that the increase of the iron concentration was barely detectable. One might have the impression that gold does play a role, but this is not fully clear. We know that Au islands on thin oxide films as substrates may be charged [16, 25] and therefore they might act as a charge source for CO_2 activation. However, in the present case the Au 4f

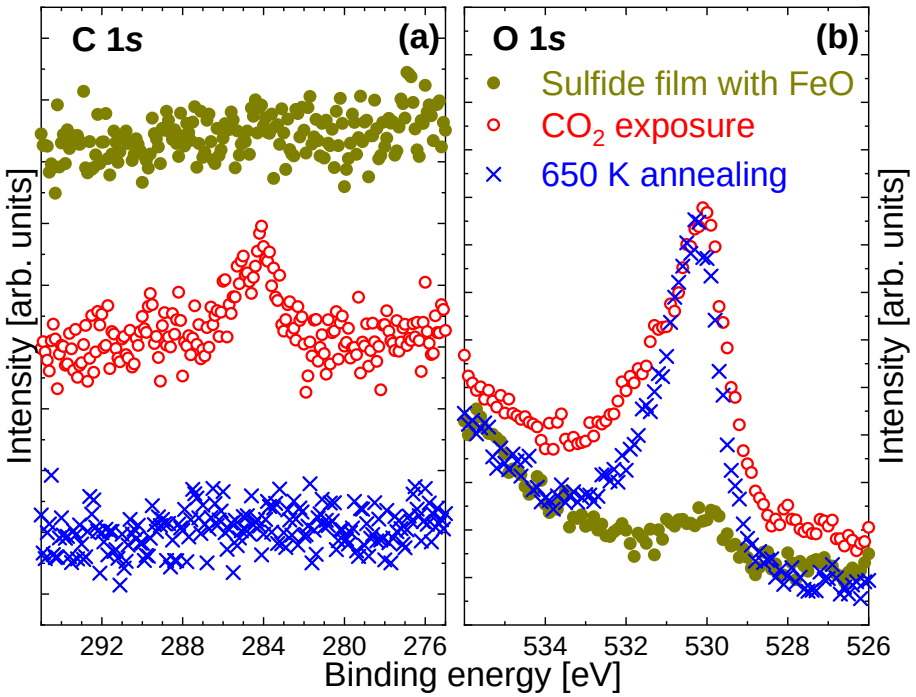

Figure 10: XPS scans in the energy regions of (a) C 1*s* and (b) O 1*s*. For clarity, the data in panel (a) are plotted with an offset along the ordinate axis.

XPS intensity did not stem from gold at the surface but either from thinning or de-wetting of the film. In the case of layer thinning there would be no direct CO_2-gold contact and in the case of de-wetting one would expect that only the gold/sulfide boundary is reactive which would make it hard to explain the observed surface concentration of CO_2 fragments unless there is spill over and catalytic action. From these considerations we might simplistically conclude that the increased iron concentration is the main reason for the increased reactivity of the sulfide layers with respect to CO_2. However, this assumption is somewhat at variance with the observation that reduction by atomic hydrogen did not activate the film surface. In this case there was also an increased iron concentration, but no CO_2 activation. There was no Au 4f intensity in the XPS spectra, and therefore the conclusion from these data would be that the presence of both gold in conjunction with iron was required for the CO_2 activation. While the relevance of an increased iron concentration in the layer is rather clear, further studies might be required to elucidate the role of the gold. These studies would have to deal with the location of the gold and the structure of the reduced surfaces. We note that a certain concentration of surface-located gold would still be compatible with our XPS data. Such gold, if it does exist, might be able to activate the surface. Finally, also thinning may lead to activation. In this case one could speculate about a charge transfer from the gold substrate to

the CO_2. It might also be that the gold signal stems from gold dissolved in the sulfide layer. However, at present these are just speculations; further studies would be needed.

5. Conclusions

We have studied the activity of well ordered iron sulfides layers on Au(111) towards CO_2 activation. As-prepared layers are not active. This is also the case for layers reduced by atomic hydrogen. Treating the surface with atomic hydrogen led to H_2S production and thus to a reduction of the sufilde, i.e. an increased iron concentration. Molecular hydrogen dosage did not have an effect at all.

We also tried to increase the iron content by deposition of additional iron (12nm). Ordering of the films required annealing at 650 K which led to a loss of the iron such that the LEED pattern became identical to what it had been before deposition, and to the appearance of a gold signal in XPS spectra. The film prepared this was way was weakly reactive.

In order to prevent iron loss into the substrate we introduced an FeO(111) diffusion blocking layer between the sulfide layer and the gold substrate. The iron sulfide layer produced in this way was not active for CO_2 activation. After adding 12 nm of iron and annealing an ordered film with increased iron content was produced. Exposure of this film to CO_2 led to 1-2 Å of CO_2-derived species at the surface showing that this surface could activate CO_2.

A relevant parameter for the activation seems to be the increased iron content, while the role of the gold is not clear. The XPS gold signal does probably stem either from de-wetted areas or from gold below the sulfide film. In both cases a direct involvement of the gold in the reaction would not be obvious. Further studies might be required to find out whether there is also gold at the surface, whether the sulfide is modified by gold in the film or whether the gold below the film is able to activate the CO_2 by charge transfer.

6. Acknowledgement

The authors would like to acknowledge the contribution of the COST Action CA17120.

Declaration of competing interest

The authors declare no competing interest.

Bibliography

[1] D. Rickard, J. W. Morse, Acid volatile sulfide (avs), Marine Chemistry 97 (3) (2005) 141–197. doi:https://doi.org/10.1016/j.marchem.2005.08.004.

URL http://www.sciencedirect.com/science/article/pii/S0304420305001039

[2] D. Rickard, G. W. Luther, III, Metal sulfide complexes and clusters, Reviews in Mineralogy and Geochemistry 61 (1) (2006) 421–504. doi:10.2138/rmg.2006.61.8.
URL http://dx.doi.org/10.2138/rmg.2006.61.8

[3] D. Rickard, G. W. Luther, Chemistry of iron sulfides, Chemical Reviews 107 (2) (2007) 514–562. doi:10.1021/cr0503658.
URL https://doi.org/10.1021/cr0503658

[4] R. Murphy, D. R. Strongin, Surface reactivity of pyrite and related sulfides, Surface Science Reports 64 (1) (2009) 1–45. doi:10.1016/j.surfrep.2008.09.002.
URL http://dx.doi.org/10.1016/j.surfrep.2008.09.002

[5] K. J. Andersson, H. Ogasawara, D. Nordlund, G. E. Brown, A. Nilsson, Preparation, structure, and orientation of pyrite FeS_2{100} surfaces: Anisotropy, sulfur monomers, dimer vacancies and a possible FeS surface phase, J. Phys. Chem. C 118 (2014) 21896–21903. doi:10.1021/jp5005924.
URL http://dx.doi.org/10.1021/jp5005924

[6] D. Santos-Carballal, A. Roldan, N. Y. Dzade, N. H. de Leeuw, Reactivity of CO_2 on the surfaces of magnetite (Fe_3O_4), greigite (Fe_3S_4) and mackinawite (FeS), Philos. Trans. R. Soc. A 376 (2110) (2018) 20170065. doi:10.1098/rsta.2017.0065.
URL http://dx.doi.org/10.1098/rsta.2017.0065

[7] T. Liu, I. Temprano, S. J. Jenkins, D. A. King, S. M. Driver, Low temperature synthesis of NH_3 from atomic N and H at the surfaces of FeS_2{100} crystals, J. Phys. Chem. C 117 (21) (2013) 10990–10998. doi:10.1021/jp308872y.
URL http://pubs.acs.org/doi/abs/10.1021/jp308872y

[8] J. Guevremont, D. Strongin, M. Schoonen, Effects of surface imperfections on the binding of CH_3OH and H_2O on FeS_2(100): using adsorbed Xe as a probe of mineral surface structure, Surf. Sci. 391 (1-3) (1997) 109–124. doi:10.1016/S0039-6028(97)00461-5.
URL http://linkinghub.elsevier.com/retrieve/pii/S0039602897004615

[9] G. Wächtershäuser, Groundworks for an evolutionary biochemistry: The iron-sulphur world, Prog. Biophys. Mol. Bio. 58 (2) (1992) 85–201. doi:10.1016/0079-6107(92)90022-X.
URL http://linkinghub.elsevier.com/retrieve/pii/007961079290022X

[10] M. Descostes, F. Mercier, N. Thromat, C. Beaucaire, M. Gautier-Soyer, Use of XPS in the determination of chemical environment and oxidation state of iron and sulfur samples: constitution of a data basis in binding energies for Fe and S reference compounds and applications to the evidence of surface species of an oxidized pyrite in a carbonate medium, Appl. Surf. Sci. 165 (4) (2000) 288–302. doi:10.1016/S0169-4332(00)00443-8.
URL http://linkinghub.elsevier.com/retrieve/pii/S0169433200004438

[11] E. M. Davis, G. Berti, H. Kuhlenbeck, V. Vonk, A. Stierle, H.-J. Freund, Growth of well-ordered iron sulfide thin films, Phys. Chem. Chem. Phys. 21 (2019) 20204–20210. doi:10.1039/C9CP04157E.
URL http://dx.doi.org/10.1039/C9CP04157E

[12] N. A. Khan, C. Matranga, Nucleation and growth of Fe and FeO nanoparticles and films on Au(111), Surf. Sci. 602 (2008) 932–942.
URL http://linkinghub.elsevier.com/retrieve/pii/S0039602807012216

[13] I. Horcas, R. Fernandez, J. M. Gomez-Rodriguez, J. Colchero, J. Gomez-Herrero, A. M. Baro, WSxM: A software for scanning probe microscopy and a tool for nanotechnology, Rev. Sci. Instrum. 78 (2007) 013705.
URL https://aip.scitation.org/doi/10.1063/1.2432410

[14] P. Feulner, D. Menzel, Simple ways to improve "flash desorption" measurements from single crystal surfaces, J. Vac. Sci. Technol. 17 (2) (1980) 662–663. arXiv:https://doi.org/10.1116/1.570537, doi:10.1116/1.570537.
URL https://doi.org/10.1116/1.570537

[15] J. T. Grant, Methods for quantitative analysis in XPS and AES, Surf. Interface Anal. 14 (6-7) (1989) 271–283. doi:10.1002/sia.740140602.
URL https://doi.org/10.1002/sia.740140602

[16] F. Calaza, C. Stiehler, Y. Fujimori, M. Sterrer, S. Beeg, M. Ruiz-Oses, N. Nilius, M. Heyde, T. Parviainen, K. Honkala, H. Häkkinen, H.-J. Freund, Carbon dioxide activation and reaction induced by electron transfer at an oxide–metal interface, Angew. Chem. Int. Ed. 54 (2015) 12484–12487. doi:10.1002/anie.201501420.

[17] NIST Chemistry WebBook, http://webbook.nist.gov/chemistry/.

[18] S. Tougaard, QUASES-Tougaard Software Package, http://www.quases.com.

[19] X. Song, E. Primorac, H. Kuhlenbeck, H.-J. Freund, Decoupling a thin well-ordered TiO_2(110) layer from a TiO_2(110) substrate with a Ti plus Ta mixed oxide interlayer, J. Phys. Chem. C 120 (15) (2016) 8185–8190. doi:10.1021/acs.jpcc.6b01318.

[20] A. Sala, H. Marchetto, Z.-H. Qin, S. Shaikhutdinov, T. Schmidt, H.-J. Freund, Defects and inhomogeneities in Fe_3O_4(111) thin film growth on Pt(111), Phys. Rev. B 86 (2012) 155430. doi:10.1103/PhysRevB.86.155430.
URL https://link.aps.org/doi/10.1103/PhysRevB.86.155430

[21] X. Weng, K. Zhang, Q. Pan, Y. Martynova, S. Shaikhutdinov, H. Freund, Support effects on CO oxidation on metal-supported ultrathin FeO(111) films, ChemCatChem 9 (4) (2017) 705–712. doi:10.1002/cctc.201601447.
URL https://doi.org/10.1002/cctc.201601447

[22] M. Ritter, W. Ranke, W. Weiss, Growth and structure of ultrathin FeO films on Pt(111) studied by STM and LEED, Phys. Rev. B 57 (1998) 7240–7251. doi:10.1103/PhysRevB.57.7240.
URL https://link.aps.org/doi/10.1103/PhysRevB.57.7240

[23] C. R. Brundle, T. J. Chuang, K. Wandelt, Core and valence level photoemission studies of iron oxide surfaces and the oxidation of iron, Surf. Sci. 68 (1977) 459–468.
URL https://doi.org/10.1016/0039-6028(77)90239-4

[24] E. Park, O. Ostrovski, J. Zhang, S. Thomson, R. Howe, Characterization of phases formed in the iron carbide process by X-ray diffraction, Mössbauer, X-ray photoelectron spectroscopy, and Raman spectroscopy analyses, Metall. Mater. Trans. B 32 (5) (2001) 839–845. doi:10.1007/s11663-001-0071-1.
URL https://doi.org/10.1007/s11663-001-0071-1

[25] C. Stiehler, F. Calaza, W.-D. Schneider, N. Nilius, H.-J. Freund, Molecular adsorption changes the quantum structure of oxide-supported gold nanoparticles: Chemisorption versus physisorption, Phys. Rev. Lett. 115 (2015) 036804. doi:10.1103/PhysRevLett.115.036804.